Sensors & Actuators: A. Physical 349 (2023) 114088

Contents lists available at ScienceDirect

Sensors and Actuators: A. Physical

journal homepage: www.journals.elsevier.com/sensors-and-actuators-a-physical

Dark background correction of the infrared detector for hyperspectral remote sensing application

Hang Zhang, Chengliang Li, Hao Xue, Chao Lin, Yuquan Zheng *

Changchun Institute of Optics, Fine Mechanics and Physics, Chinese Academy of Sciences, Changchun 130033, China

ARTICLE INFO

Keywords:
Dark current
Long-wave infrared
Multiframe superposition
Noise equivalent temperature difference

ABSTRACT

The dark current is one of the main factors that influences the performance of infrared photodetectors, as it restricts the integration time and decreases the signal-to-noise ratio of an imaging system. Especially for hyperspectral remote sensing applications, the dark background occupies most of the dynamic range, owing to the narrow bandwidth and weak incident energy of each spectral channel. A general method for suppressing the dark current is to keep the optical system and the focal plane array (FPA) at an extremely low temperature (less than 30 K). However, maintaining a low temperature consumes a large amount of energy. Here, we present one correction method to eliminate the influence of the dark current on image quality. According to the real-time FPA temperature, the instantaneous dark background of each pixel is calculated and subtracted from the original image. Moreover, multiframe superposition is employed to improve the performance of the infrared hyperspectral imager. Based on this correction method, the noise equivalent temperature difference (NETD) in the imaging system is better than 0.3 K after 32 frames are merged.

1. Introduction

HgCdTe infrared detectors and technologies have long-term interest in a wide-ranging applications such as night vision, infrared sensing and imaging. This material has the following advantages: highly tunable bandgap, high detection sensitivity, high mobility of electron and low dielectric constant, etc [1–4]. However, because the dark current is relatively high, the integrated capacitor often reaches the pixel saturation point before the required time for the integration [4]. How to reduce the influence of dark background on the detector has been a hot and important research topic. Generally, there are two ways: (1) Active method: the optical system and the FPA are maintained at extremely low temperatures to suppress the dark background. (2) Passive method: the dark background of each pixel is estimated in real time and subtracted from the original image in imaging processing [5,6]. Passive methods consist of two approaches: “dark frame correction” and “dark pixel correction”. For dark frame correction, a dark frame is obtained from an exposure with a closed shutter immediately before or after the light exposure [7,8]. In contrast, for dark pixel correction, a dark pixel is shielded from the target radiation and responds only to the dark current in the FPA and the background radiation of the instrument. The estimated dark current of each pixel is calculated based on the dark frame or dark pixel and is subtracted from the original image to realize dark current correction [9,10]. In both of these approaches, an intermediate link is introduced, resulting in greater correction error.

Near-Earth Object (NEO) Surveyor, a NASA planetary defense space mission, is currently in Phase B, with a planned launch date in 2026. NEO Surveyor will employ eight passively cooled HgCdTe Sensor Chip Assemblies (SCAs) across two bands, covering 4–5.2 μm at an SCA temperature of 57 K and 6–10 μm at 40 K [11,12]. The Mid-infrared Airborne Hyperspectral Imager (MAHI) instrument is a moderate-swath high-spectral-resolution imaging spectrometer that spans the 3.3–5.4 μm MWIR region in 640 contiguous channels. The temperatures of the detector and the optics are both 77 K [13]. The Mineral and Gas Identifier (MAGI) is a wide-swath moderate-spectral-resolution thermal infrared imaging spectrometer that spans the spectral window of 7.1–12.7 μm in 32 uniform and contiguous channels. The detector temperature is 55 K, and the optics temperature is 120 K [14]. The Spitzer space telescope includes three infrared instruments: IRAC, IRS, and MIPS. They share a common FPA temperature, which was initially 8 K due to cooling by a liquid helium cryostat. Since the exhaustion of the cryogens, the space telescope’s FPAs have equilibrated to approximately 27 K [15–17].

This paper is based on the infrared hyperspectral imager from one

* Corresponding author.
E-mail addresses: hangzhang@ciomp.ac.cn (H. Zhang), zhengyq@sklao.ac.cn (Y. Zheng).

https://doi.org/10.1016/j.sna.2022.114088
Received 22 October 2022; Received in revised form 30 November 2022; Accepted 9 December 2022
Available online 10 December 2022

Table 1
The key parameters of this LWIR detector.

Parameter	Value
Spectral range	8.5–12.5 μm
Average peak detection rate	5×10^{10} cmHz$^{1/2}$W^{-1}
Readout noise	1500 e-
Dark current	2 nA
Full well capacity	37 Me-
Operating temperature	60 K
Cooling power consumption	45 W

advanced research project of China in the geostationary orbit. The FPA is cooled to approximately 60 K by a Stirling cycle cooler. One novel method for correcting the dark background based on the FPA temperature is presented, and multiframe superposition is employed to improve the NETD. The project overview is introduced and the relationship between the dark background and the FPA temperature is presented in the section2. The Section 3 describes that how to eliminate dark background fluctuations. The effect of the new method is showed by comparing different correction techniques in the Section 4.

2. Relationship between the dark background and temperature

"The Study for Full-spectrum and Hyper-spectrum Detection on the Geostationary Orbit" is one advanced research aerospace project funded by Chinese Academy of Sciences. This mission consists of visible-near infrared (VNIR), short-wave infrared (SWIR), medium-wave infrared (MWIR) and long-wave infrared (LWIR) four hyperspectral imagers, covering the spectral range from 0.3 μm to 12.5 μm. This paper focuses on the LWIR spectrometer. The spectral rang is 8.5 μm to 12.5 μm, and the NETD requirement of the whole LWIR system is less than 0.5 K. The FPA of a HgCdTe detector consists of photodiode arrays with 320 × 256 pixels at a 30 μm pixel pitch. The parameters of the long-wave detector are listed in Table 1.

The bandwidth of each spectral channel is usually very narrow for the hyperspectral imager, 120 nm for the LWIR spectrometer in the paper. In order to compensate the weak incident energy of one single spectral channel, integration time increment and multiframe superposition are often employed. This LWIR detector is operated at an FPA temperature of 60 K, and the dark current is 2 nA. The dynamic range is occupied by the dark current components to a large extent, which limits the increase in the integration time. Moreover, the multiframe superposition effect worsens due to the fluctuation of the dark current over time. Dark backgrounds with different pixels and at different time need to be obtained and eliminated [18].

Although the FPA temperature is controlled at approximately 60 K, the small temperature fluctuations can cause considerable variations in the dark background. A temperature measuring diode, constant-current source and 32 bit analog-to-digital converter are selected to measure the FPA temperature accurately, and multiple sampling is applied to eliminate the random noise. Measurement frequency is 250 times/s, which is higher than imaging frequency. The relationships between the dark background and FPA temperature for different pixels are shown in Fig. 1. Test condition: the temperature of the optical system is maintained at 120 K, the entrance pupil is shielded from the target radiation by a cold stop. The frame rate is set to 100 frames/s and the integration time is set to 2.5 ms.

Four pixels are chosen arbitrarily at the different locations of the 2D detector, horizontal axis represents the frame number. Firstly, it can be seen that the dark backgrounds of different pixels vary considerably, and the dark background output rises with the increasing wavelength. Secondly, although the variation range of the FPA temperature is only 0.02 K, the dark background output is highly consistent with the FPA temperature in terms of peaks and troughs. Finally, the temperature curves has time delay of 200 ms comparing with the dark background. We need to correct the dark background on the time dimension

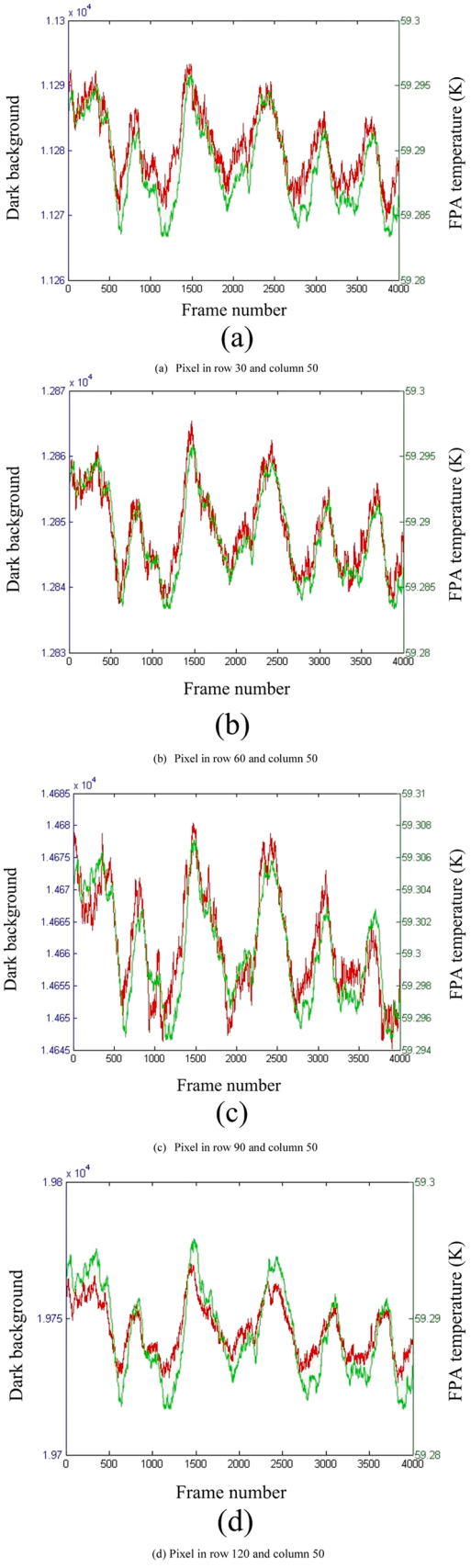

Fig. 1. The relationships between the dark background and the FPA temperature for different pixels. The green lines show the DN value of the dark background (left axis), the red lines show the FPA temperature (right axis).

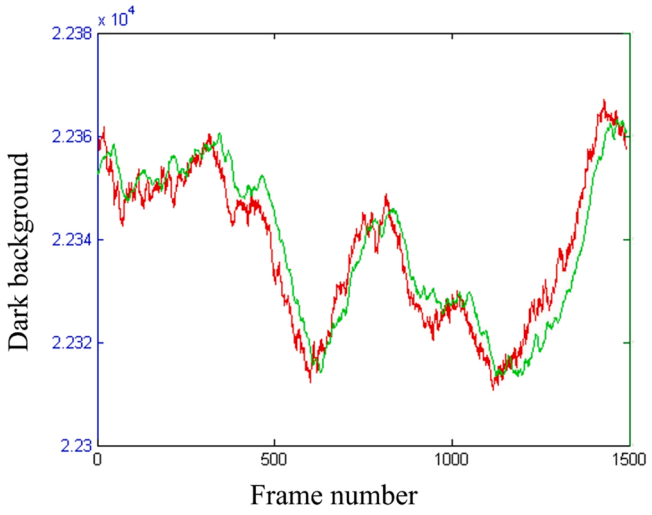

Fig. 2. Comparison between the measured value of dark background (red line) and the estimated one derived from the FPA temperature (green line).

(fluctuation over time) and the spatial dimension (differences between pixels).

3. Dark background correction

According to the comparison between the dark background and FPA temperature as shown in Fig. 1. We can use the FPA temperature to simulate the dark background fluctuations over time. The nonuniformity between different pixels is also needed to be corrected. Linear least square fitting to the temperature for each pixel is implemented, and a set of coefficients is derived for each pixel [19].

$$D(i,j,n) = a(i,j) * T(n) + b(i,j) \tag{1}$$

Where $a(i,j)$ and $b(i,j)$ is the coefficients of the pixel in row i and column j, $T(n)$ is the FPA temperature of the nth frame, $D(i,j,n)$ is the estimated value of dark background of the pixel in row i and column j derived from the FPA temperature of the nth frame.

For more accurate fitting, the change trend at large time scales is focused and the random noise is ignored. A moving average model is employed on the dark background and the temperature. In order to verify the fitting results, the measured value and estimated value of the

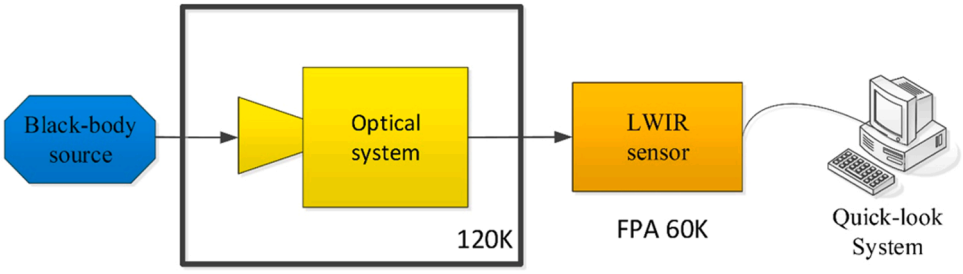

Fig. 3. The block diagram of the testing system for NETD.

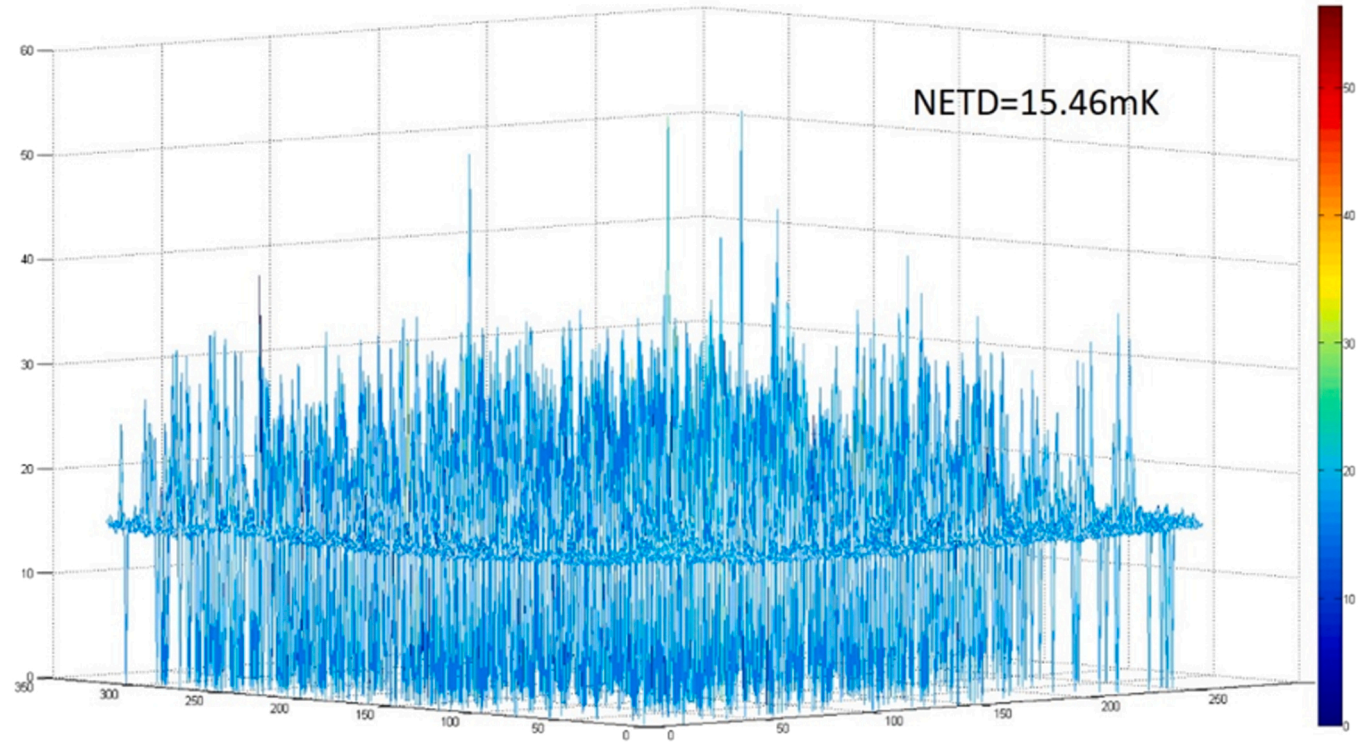

Fig. 4. the NETD of the LWIR detector without the optical system, the x- and y-axes represent different pixels, and z-axis represents the NETD of the corresponding pixel. The average value of NETDs is 15.46 mK.

dark background from one new set of image data are compared as shown in Fig. 2.

This result is consistent with the results shown in Fig. 1, the estimated dark background curves simulated according to the FPA temperature are 200 ms behind the measured curves. The temperature measurement frequency is 250 times/s, which is higher than the imaging frequency. Therefore, this delay is not caused by insufficient sampling but by heat conduction from the FPA to the diode. This delay can be corrected by the linear fitting parameters.

4. Correction result

The most common performance parameter for infrared instruments is NETD. In this section, the NETD of the imaging system is measured to verify the dark background correction effect. Fig. 3 provides the block diagram of the testing system. An area array blackbody is used as the target source, and the temperature stability is better than 0.1 K, providing uniform radiation on the pixels of the infrared FPA [20,21].

The testing procedures are described as follows:

1) The testing system is connected correctly as shown in Fig. 3. Optical system is placed in the vacuum environment, whose temperature is maintained at 120 K to reduce the instrument radiation.
2) The Stirling cycle cooler is powered on, the imaging system doesn't operate until the FPA temperature is stabilized at 60 K.
3) The blackbody temperature is set to 293 K and 308 K respectively, 5000 frames data of image is stored for each temperature, considering the need of multiframe superposition. In addition, the entrance pupil is shielded and the integration time remain unchanged, 2000 frames data of dark background is stored.

NETD can be calculated according to Eqs. 2 and 3:

$$NETD(\mathrm{i,j}) = \frac{T - T_0}{(V_S(i,j)/V_N(i,j))} \tag{2}$$

$$V_S(\mathrm{i,j}) = \frac{1}{F}\sum_{f=1}^{F} V_{DS}[(i,j),T,f] - \frac{1}{F}\sum_{f=1}^{F} V_{DS}[(i,j),T_0,f] \tag{3}$$

Where T is 308 K, T_0 is 293 K, $V_S(i,j)$ is the difference value between the average of all frame images with the blackbody temperature of 293 K and 308 K for the pixel in row i and column j. $V_N(i,j)$ is the root mean square (RMS) value of all frame images for the pixel in row i and column j at 293 K.

According to the above equation, the NETD of the LWIR detector is calculated without optical system. Due to no spectroscopic system, all pixels receive the radiation flux with the spectral range from 8.5 μm to 12.5 μm, the integration time is set to 40 μs, the dark current has little impact on the detector output.

Next, the NETD of the whole system is measured, including the spectroscopic system. The hyperspectral imager has dozens of spectral channels, the radiation from the target is being split to narrow bands, resulting in very weak incident radiation for each pixel. The integration time needs to be increased to increase the radiation flux. However, as the integration time increases, the influence of the dark current becomes more apparent, and the NETD in a single image frame worsens. Multiframe superposition is commonly implemented to improve the NETD. The fluctuation in the dark background between different frames reduces the multiframe superposition effect because multiframe superposition reduces only the impact of white noise [22,23]. When white noise is the dominant noise component, the NETD in the average frame is close to the theoretical value. It is assumed that M frames are merged. Fig. 4.

$$NETD_M = \frac{NETD}{\sqrt{M}} \tag{4}$$

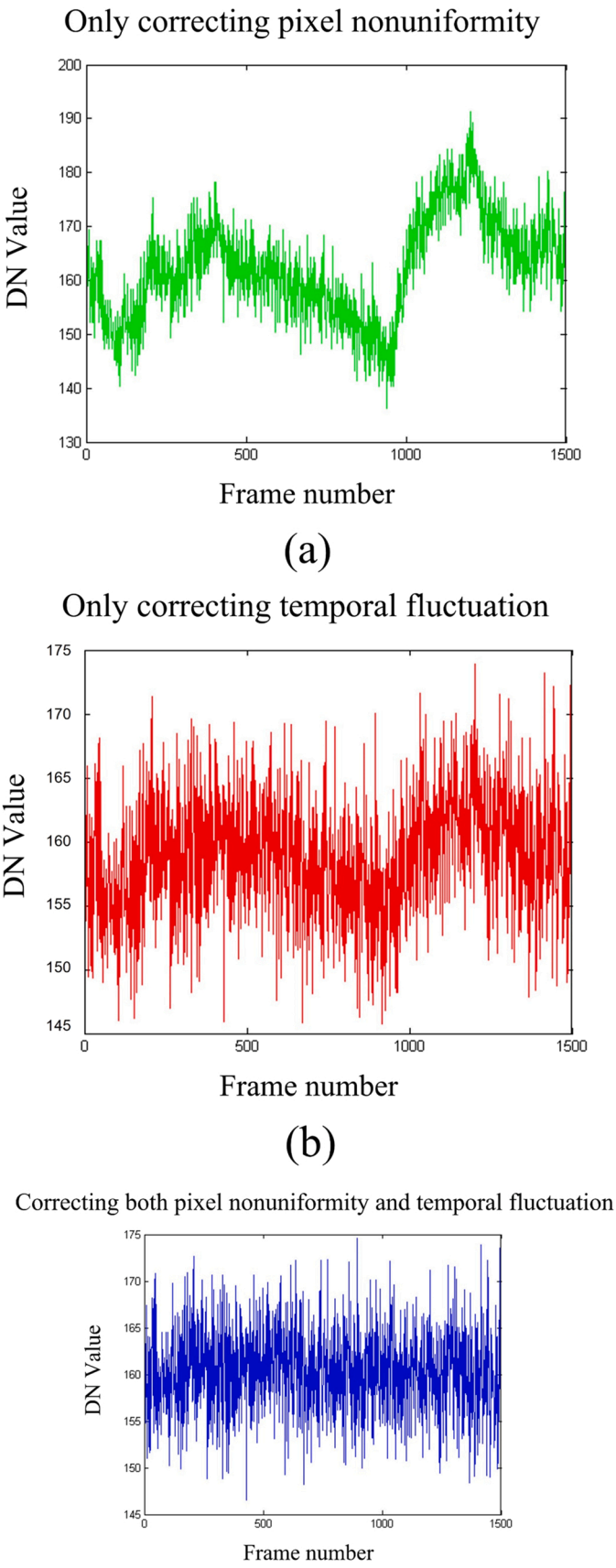

Fig. 5. The valid signal after dark background correction with three techniques.

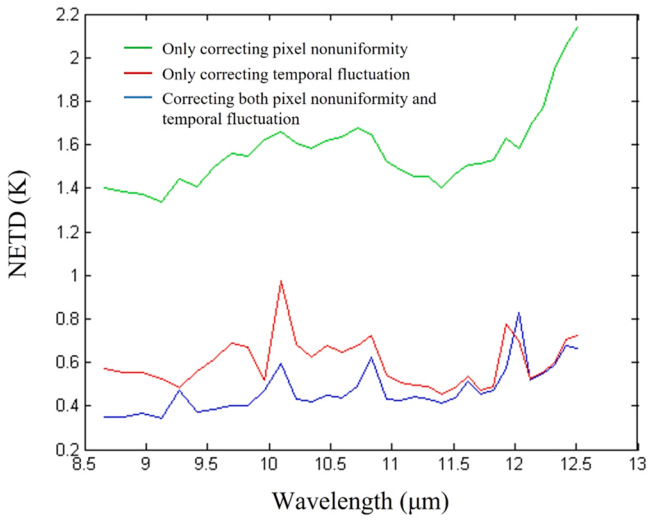

Fig. 6. The measured NETD of the whole system after dark background correction with the three techniques.

Therefore, suppressing the fluctuation of dark background on time domain is significant to improve the NETD of the imaging system for the infrared spectrum. There are two directions to eliminate the dark background noise, the first one is to maintain the temperatures of the optics and the FPA at extremely low level, this method can suppress the generation of the dark current fundamentally. However, it needs to consume a lot of resources and can not be sustained. The second direction (the main research contents in this paper) is to estimate the dark backgrounds of different pixels in real time and subtract them from the original image according to a limited number of information. Here, three techniques to estimate the dark backgrounds of different pixels are compared. For the first one, only the nonuniformity between pixels is corrected and the fluctuation of dark background over time is ignored. The entrance pupil is shielded from target radiation by a cold stop, several frames of the dark background are stored and averaged as dark reference. The second technique is contrary to the first one, the fluctuation of dark background over time is corrected and the nonuniformity between pixels is ignored. The average output of pixels in one line at the edge of the FPA is used as the dark reference for the current frame, this line of pixels is located outside the range of the target radiation and responds only to the dark current and instrument radiation. For the third one, the fluctuation of dark background over time and nonuniformity between pixels are both corrected. Before imaging, plenty of dark background frames are obtained and the FPA temperatures of each frame are recorded simultaneously. The relationship between the dark background and the FPA temperature is expressed with the linear fitting, a set of coefficients is obtained for each pixel. The estimated dark background of the corresponding pixel can be calculated according to its coefficients and the current FPA temperature. During the imaging process, the estimated dark background, as the dark reference, is subtracted from the original image.

A uniform blackbody at 293 K acts as the radiation source. Fig. 5 illustrates the valid signal after dark background correction with three techniques, taking the pixel in row 100 and column 100 as an example.

It can be seen that the noticeable fluctuation noise remains after only pixel nonuniformity correction with the first technique. The fluctuation of valid signal in time domain can be eliminated mostly through the second technique, only tiny fluctuation remains. The third technique has a more obvious effect compared to the second one, leaving only shot noise after correction.

Taking the pixels in the column 35 as an example, the measured NETD of the whole LWIR system is shown in Fig. 6, and the three techniques are compared with the spectral range from 8.5–12.5 μm.

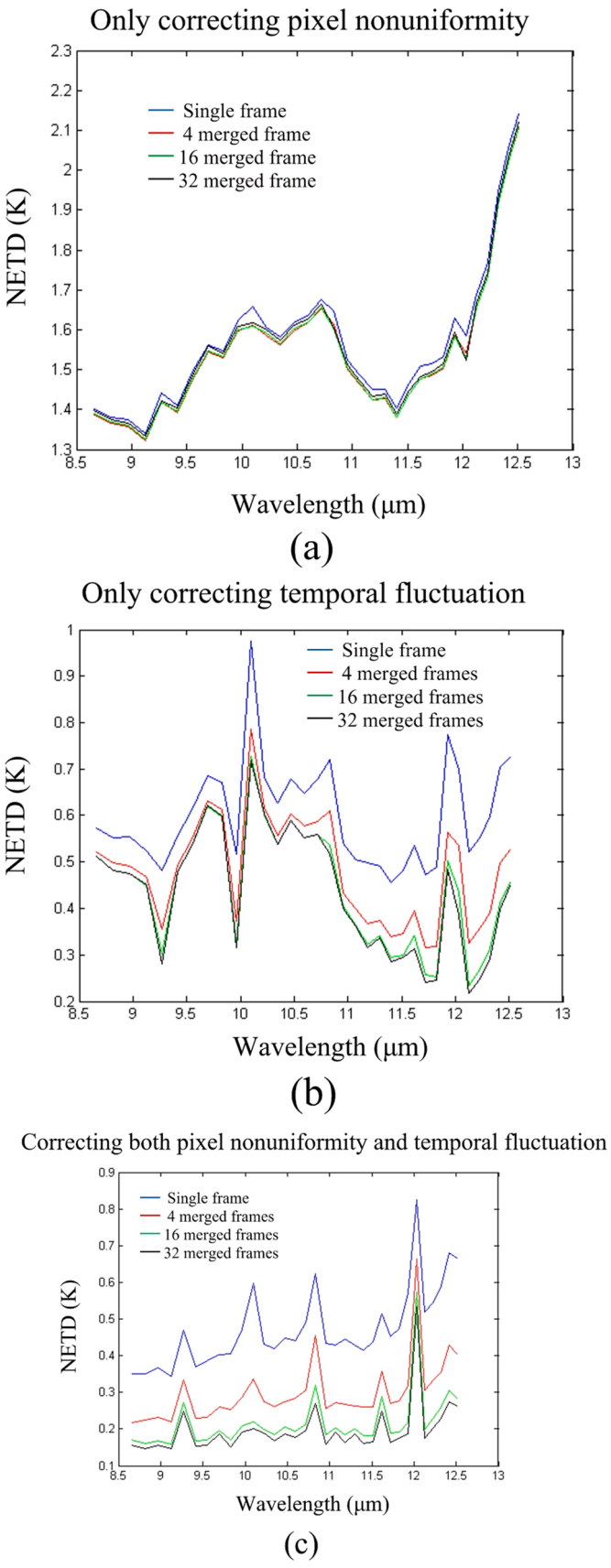

Fig. 7. The influence of multiframe superposition on NETD improvement with the three techniques.

This result is consistent with the results in Fig. 5, and the NETD has the worst value after only pixel nonuniformity is corrected. The NETD value is the best after correcting both pixel nonuniformity and temporal fluctuations. In addition, the NETD after only temporal fluctuations are corrected is satisfactory but is slightly different than the best result. The influence of multiframe superposition on NETD improvement with the three technique is discussed below.

The multiframe superposition effect is least apparent after only pixel nonuniformity correction (the first technique). It is because that multiframe superposition can reduce only the white noise components. However, there is still plenty of fluctuation noise over time with the first technique, and the white noise is not the dominant type of noise in the system. The effect is most apparent after both pixel nonuniformity correction and temporal fluctuation correction (the third technique). Especially for 4 frames merging, the result is close to the theoretical limit. The reason is that this technique can eliminate the dark background noise almost completely, leaving only shot noise (white noise). In addition, as the number of merging frame increases, the proportion of white noise is decreasing and multiframe superposition effect is less and less apparent. After 32 frames merged, the NETD is almost no longer improved.Fig. 7.

5. Conclusion

The dark background is the main factor that affects the performance of infrared imaging system, especially for LWIR spectra. Accurate dark background correction can improve the NETD and increase the dynamic range significantly for the whole system. Based on an LWIR hyperspectral imager with the spectral range from 8.5 μ to 12.5 μm, the relationship between the dark background and FPA temperature is exactly determined in this paper. Three dark background correction techniques are introduced to address pixel nonuniformity and temporal fluctuation noise. The effects of the three correction techniques are compared to evaluate the contribution of different factors to background noise. Finally, the NETD values of the single frame mode and multiframe superposition mode are measured to verify the applicability of the new correction method. The results of this research can provide a theoretical basis for improving the image quality of the subsequent LWIR hyperspectral imager.

CRediT authorship contribution statement

Hang Zhang: (the first author): Conceptualization, Methodology, Writing – original draft. **Chengliang Li:** Software, Formal analysis. **Hao Xue:** Data curation. **Chao Lin:** Validation. **Yuquan Zheng:** (the corresponding author): Funding acquisition, Supervision.

Declaration of Competing Interest

The authors declare that they have no known competing financial interests or personal relationships that could have appeared to influence the work reported in this paper.

Data Availability

The authors do not have permission to share data.

Acknowledgement

The work was supported by the Natural Science Foundation of Jilin Province, China [grant number 20200201203JC] and the National Key Research and Development Program of China [grant number 2016YFB0500300].

References

[1] C. Ailiang, L. Lingfeng, S. Changhong, D. Ruijun, H. Li, Y. Zhenhua, Analysis of dark current generated by long-wave infrared, Infrared Phy. Technol. vol. 103 (2019), https://doi.org/10.1016/j.infrared.2019.103036.
[2] L. Zhu, et al., Low frequency noise-dark current correlations in HgCdTe infrared photodetectors, Opt. Express vol. 28 (16) (2020) 23660–23669, https://doi.org/10.1364/OE.399565.
[3] L. Balick, A. Gillespie, A. French, I. Danilina, J.-P. Allard, A. Mushkin, Longwave thermal infrared spectral variability in individual rocks, IEEE Geosci. Remote Sens. Lett. vol. 6 (1) (2009) 52–56, https://doi.org/10.1109/lgrs.2008.2006005.
[4] A. Dehzangi, J. Li, M. Razeghi, Band-structure-engineered high-gain LWIR photodetector based on a type-II superlattice, Light Sci. Appl. vol. 10 (1) (2021) 17, https://doi.org/10.1038/s41377-020-00453-x.
[5] L. Yang et al., "Dark current mechanism of medium wave HgCdTe avalanche photodiode," presented at the 24th National Laser Conference & Fifteenth National Conference on Laser Technology and Optoelectronics, 2020.
[6] T. O'Brien, E. Boss, Correction of radiometry data for temperature effect on dark current, with application to radiometers on profiling floats, Sensors vol. 22 (18) (2022), https://doi.org/10.3390/s22186771.
[7] W.C. Porter et al., "Dark current measurements in a CMOS imager," presented at the Sensors, Cameras, and Systems for Industrial/Scientific Applications IX, 2008.
[8] P. Wiegand et al., "Method of dark current correction in spectrometer, involves subtracting dark exposure from light exposures and storing result as accumulation and summing or averaging N accumulations to generate result," U.S. Patent US2018328785-A1, Nov. 15, 2018.
[9] B. Ma et al., "A new method of CCD dark current correction via extracting the dark Information from scientific images," presented at the High Energy, Optical, and Infrared Detectors for Astronomy VI, 2014.
[10] T. O'Brien, E. Boss, Correction of radiometry data for temperature effect on dark current, with application to radiometers on profiling floats, Sensors vol. 22 (18) (2022), https://doi.org/10.3390/s22186771.
[11] N. Reilly, et al., Testing results from pathfinder HgCdTe infrared detectors for the near-earth object surveyor mission," presented at the X-Ray, Opt., Infrared Detect. Astron. X (2022).
[12] G.R. Zengilowski, et al., Modulation transfer function measurements of HgCdTe long wavelength infrared arrays for the near-earth object surveyor, J. Astron Telesc. Inst. vol. 8 (1) (2022), https://doi.org/10.1117/1.Jatis.8.1.016002.
[13] D.M. Tratt, et al., MAHI: An airborne mid-infrared imaging spectrometer for industrial emissions monitoring, IEEE Trans. Geosci. Remote Sens. vol. 55 (8) (2017) 4558–4566, https://doi.org/10.1109/tgrs.2017.2693979.
[14] J.L. Hall, et al., MAGI: a new high-performance airborne thermal-infrared imaging spectrometer for earth science applications, IEEE Trans. Geosci. Remote Sens. vol. 53 (10) (2015) 5447–5457, https://doi.org/10.1109/tgrs.2015.2422817.
[15] C.W. McMurtry, H.A. MacEwen, J.L. Pipher, W.J. Forrest, M.W.M. de Graauw, "Spitzer space telescope: dark current and total noise prediction for InSb detector arrays in the infrared array camera (IRAC) for the post-cryogen era," presented at the Space Telescopes and Instrumentation I: Optical, Infrared, and Millimeter, 2006.
[16] W.A. Mahoney et al., "Spitzer warm mission transition and operations," presented at the Observatory Operations: Strategies, Processes, and Systems III, 2010.
[17] R. Tian, et al., Chip-integrated van der Waals PN heterojunction photodetector with low dark current and high responsivity, Light Sci. Appl. vol. 11 (1) (2022) 101, https://doi.org/10.1038/s41377-022-00784-x.
[18] Y. Zhou, et al., Ultra-broadband metamaterial absorbers from long to very long infrared regime, Light Sci. Appl. vol. 10 (1) (2021) 138, https://doi.org/10.1038/s41377-021-00577-8.
[19] X. Han, et al., Dark current and noise analysis for Long-wavelength infrared HgCdTe avalanche photodiodes, Infrared Phy. Techno. vol. 123 (2022), 104108, https://doi.org/10.1016/j.infrared.2022.
[20] N.I. Iakovleva, The study of dark currents in HgCdTe heterostructure photodiodes, J. Commun. Technol. El+. vol. 66 (3) (2021) 368–374, https://doi.org/10.1134/s1064226921030220.
[21] Y. Chang, L. Yan, L. Liu, H. Fang, S. Zhong, Infrared aerothermal nonuniform correction via deep multiscale residual network, IEEE Geosci. Remote Sens. Lett. vol. 16 (7) (2019) 1120–1124, https://doi.org/10.1109/lgrs.2019.2893519.
[22] C. McMurtry, et al., Development of sensitive long-wave infrared detector arrays for passively cooled space missions, Opt. Eng. vol. 52 (9) (2013), https://doi.org/10.1117/1.Oe.52.9.091804.
[23] A. Hecht, A. Reinhardt, C. Bradley, P. McManamon, M.D. Turner, G.W. Kamerman, "Thermal drift compensation in dark-frame non-uniformity correction for an InGaAs PIN 3D flash lidar camera," presented at the Laser Radar Technology and Applications XXVI, 2021.

Hang Zhang received the Ph.D. degree in Jilin University in 2017. He is an associate researcher at the Changchun Institute of Optics, Fine Mechanics and Physics, Chinese Academy of Sciences. His research interests include infrared imaging system and image processing.

Chengliang Li received the Ph.D. degree in optical engineering from the Changchun Institute of Optics, Fine Mechanics and Physics (CIOMP), Chinese Academy of Sciences in 2021. He is an associate researcher at CIOMP. His research is focused mainly on the mechanical design and analysis of spectrometers.

Hao Xue received the Master degree in mechanical electronic engineering from Harbin institute of technology, Harbin, China, in 2013. He is an assistant researcher at the Changchun Institute of Optics, Fine Mechanics and Physics, Chinese Academy of Sciences. His research is focused mainly on the structure design of spectrometer.

Chao Lin received the Master degree in mechanical engineering from Jilin University in 2009. He is a researcher at the Changchun Institute of Optics, Fine Mechanics and Physics, Chinese Academy of Sciences. His research is focused mainly on the spectrograph calibration.

Yuquan Zheng received the Ph.D. degree in optical engineering from the Changchun Institute of Optics, Fine Mechanics and Physics (CIOMP), Chinese Academy of Sciences in 1999. He is an researcher at CIOMP. His research is focused mainly on the hyperspectral imaging technology and optical system design.